Available online at www.sciencedirect.com
SCIENCE DIRECT®
Icarus 183 (2006) 101–114
ICARUS
www.elsevier.com/locate/icarus

The size–frequency distribution of dormant Jupiter family comets

Kathryn Whitman [a], Alessandro Morbidelli [b], Robert Jedicke [a,*]

[a] *Institute for Astronomy, University of Hawaii, 2680 Woodlawn Dr., Honolulu, HI 96822, USA*
[b] *Observatory of Nice, B.P. 4229, 06304 Nice Cedex 4, France*

Received 17 May 2005; revised 23 December 2005

Available online 24 April 2006

Abstract

We estimate the total number and the slope of the size–frequency distribution (SFD) of dormant Jupiter family comets (JFCs) by fitting a one-parameter model to the known population. We first select 61 near-Earth objects (NEOs) that are likely to be dormant JFCs because their orbits are dynamically coupled to Jupiter [Bottke, W.F., Morbidelli, A., Jedicke, R., Petit, J., Levison, H.F., Michel, P., Metcalfe, T.S., 2002a. Icarus 156, 399–433]. Then, from the numerical simulations of Levison and Duncan [1997. Icarus 127, 13–32], we construct an orbit distribution model for JFCs in the NEO orbital element space. We assume an orbit-independent SFD for all JFCs, the slope of which is our unique free parameter. Finally, we compute observational biases for dormant JFCs using a calibrated NEO survey simulator [Jedicke, R., Morbidelli, A., Spahr, T., Petit, J., Bottke, W.F., 2003. Icarus 161, 17–33]. By fitting the biased model to the data, we estimate that there are ∼75 dormant JFCs with $H < 18$ in the NEO region and that the slope of their cumulative SFD is -1.5 ± 0.3. Our slope for the SFD of dormant JFCs is very close to that of active JFCs as determined by Weissman and Lowry [2003. Lunar Planet. Sci. 34. Abstract 2003]. Thus, we argue that when JFCs fade they are likely to become dormant rather than to disrupt and that the fate of faded comets is size-independent. Our results imply that the size distribution of the JFC progenitors—the scattered disk trans-neptunian population—either (i) has a similar and shallow SFD or (i′) is slightly steeper and physical processes acting on the comets in a size-dependent manner creates the shallower active comet SFD. Our measured slope, typical of collisionally evolved populations with a size-dependent impact strength [Benz, W., Asphaug, E., 1999. Icarus 142, 5–20], suggests that scattered disk bodies reached collisional equilibrium inside the protoplanetary disk prior to their removal from the planetary region.

Keywords: Comets; Asteroids

1. Introduction

The populations of small bodies in the Solar System provide an important key to unlocking its birth and evolution. The constituent materials of comets can be explored through spectroscopic observations, while their dynamical and physical history can be extracted from studies of their orbital and size–frequency distribution.

Several studies have traced the dynamical evolution of comets from their parent reservoirs (the scattered disk for Jupiter family comets, the Oort cloud for long-period comets) to their ultimate ejection from the Solar System (Weissman, 1978; Fernandez, 1981; Levison and Duncan, 1997; Wiegert and Tremaine, 1999). The orbital distribution of comets that these studies predict is different from the observed distribution. In general, there is a deficit of comets on dynamically evolved orbits, which is usually interpreted as an indication that comets *fade* with age: comets appear to be active only over a limited number of revolutions with small perihelion distance.

Curiously, Jupiter family comets (JFC) and long-period comets (LPC) appear to follow very different fading laws. The JFCs are active over a lifetime of about 10,000 y or ∼1000 revolutions (Levison and Duncan, 1997) while the LPCs disappear much faster. Only 10% of the LPCs survive more than 50 passages to small perihelion, while only 1% of them survives more than 2000 passages (Wiegert and Tremaine, 1999).

The fate of faded comets is still a subject of debate. Do comets disintegrate into small, undetectable pieces (like in the case of Comet LINEAR C/2001 A2) or do they develop an insulating crust that prevents or restricts further outgassing allowing them to survive as inactive (dormant or extinct) bodies with an

* Corresponding author.
E-mail address: jedicke@ifa.hawaii.edu (R. Jedicke).

0019-1035/$ – see front matter
doi:10.1016/j.icarus.2006.02.016

asteroidal appearance? In this respect, JFCs and LPCs seem to behave differently. Bottke et al. (2000, 2002a) concluded that about $6 \pm 4\%$ of the population of near-Earth objects (NEOs) is composed of extinct JFCs. Recent spectral observations of NEOs (Fernández et al., 2001; Binzel et al., 2004) corroborate this result. This implies that a substantial fraction of JFCs orbit the Sun as inactive bodies. Conversely, Levison et al. (2002) showed that the population of dormant LPCs is only about 1% of the total expected population if it is assumed that LPCs fade rather than disrupt. In other words, 99% of LPCs disintegrate when they disappear.

The papers by Bottke et al. (2000, 2002a) were not devoted to characterizing the population of extinct JFCs. The authors created an orbital distribution model for the overall NEO population by combining the characteristic distributions of objects coming from 5 possible source regions: 4 sources belonging to the main asteroid belt, plus the JFCs. Each source population was assumed to have the same absolute magnitude (H) distribution. The relative importance of the sources, as well as the slope of the H-distribution, were determined by the best fit to the distribution of the NEOs detected by the Spacewatch survey (138 objects). Their results concerning JFCs were hampered by small number statistics since the Spacewatch sample included only a handful of dormant comet candidates. In particular, the NEO H-distribution determined by Bottke et al. (2000, 2002a) does not necessarily characterize the dormant JFC population.

The size–frequency distribution (SFD) of dormant comets is important to understanding the fading issue. It can be related to the H frequency distribution (HFD) and to the mass distribution (MFD) through a simple calculation if one assumes that the objects have a size-independent albedo and density (Durda, 1993). Since other researchers have determined the SFD or MFD we provide the conversion for the reader's convenience. A cumulative H-distribution of the form

$$N(< H) \propto 10^{\alpha H} \tag{1}$$

is strictly equivalent to a cumulative size distribution of the form

$$N(> D) \propto D^{-5\alpha}, \tag{2}$$

where D is the diameter, or to a cumulative mass distribution of the form

$$N(> M) \propto M^{-5\alpha/3}, \tag{3}$$

where M is the mass. Note that the exponent of the differential and cumulative HFD are identical while the exponent for the differential distributions in size and mass become $-5\alpha - 1$ and $-5\alpha/3 - 1$, respectively. We prefer to work with the H-distribution because it is directly related to the observations (the apparent brightness of an object is usually measured, not its size or its mass).

In a reservoir of small bodies in collisional equilibrium, like the asteroid belt or the Kuiper belt, and if the strength of objects is independent of their size (a Self-Similar Collision Cascade; e.g., Tanaka et al., 1996), then the population is expected to have a SFD with $\alpha = 0.5$ (e.g., Dohnanyi, 1969). In reality, the SFD or H-distribution has a wavy aspect such that the value of α for the main belt (MB) asteroids is size-dependent with a value that jumps around the theoretically expected value (e.g., Ivezić et al., 2001; Jedicke and Metcalfe, 1998; van Houten et al., 1970; Kuiper et al., 1958). There are a variety of explanations for the variation of α about the theoretical value, including it being

(a) a relic of the primordial SFD for the larger asteroids (e.g., Bottke et al., 2005),
(b) a consequence of a size-dependent strength of asteroids (e.g., Durda et al., 1998),
(c) due to the quick removal of very small dust particles that eliminates the tiny tail of the population that wags the rest of the SFD (e.g., Campo Bagatin et al., 1994).

The actual SFD is probably a result of a combination of all these proposed mechanisms and an accurate measure of the SFD of MB asteroids over all size ranges may allow the effects to be disentangled.

The near-Earth objects (NEOs) are expected to mimic the wavy SFD of their source region, the main belt, but to have a larger slope because the main process that transports main belt objects into the NEO region—the Yarkovsky effect (Bottke et al., 2002b)—is size-dependent. This has been verified for NEOs with $H < 18$ by Morbidelli and Vokrouhlický (2003).

For active comets, the SFD may be further complicated by a size-dependent fading law. Moreover, the comparison between the SFD of the dormant population with that of the active population can tell us whether the probability of disintegrating versus becoming dormant is size-dependent. The comparison between the SFDs of dormant comet populations that have very different fading laws can also be very instructive. Unlike NEOs, comets originate in reservoirs that might not be in collisional equilibrium. Indeed comets, once stored in the scattered disk or in the Oort cloud, might have avoided collisions due to the huge volume available in these reservoirs.

In this paper, taking advantage of the fact that several dozen NEOs have been recently discovered on orbits that are typical of JFCs, we wish to reassess the issue of the total number of dormant JFCs and of their SFD. In Section 2 we explain the general principle of our method. In particular, we explain how we select the candidate dormant JFCs from the NEO catalogue (Section 2.1), how we construct an orbital distribution model (Section 2.2), how we estimate the observational biases (Section 2.3) and how we determine the best fit value of α (Section 2.4). In Section 3 we compare our best fit model with the observed population in terms of orbital and absolute magnitude distributions. We evaluate the statistical agreement between model and observations (Section 3.1), and we discuss the dependence of the results on the selected candidate JFC population and the systematic errors in our measurement (Section 3.2 and Section 3.3, respectively). In Section 4 we finally discuss the interesting implications of our results.

2. Method

Any set of observed objects is a convolution of the actual underlying population and the methods and instrumentation used to detect them. In the case of dormant JFCs currently on NEO orbits, the observed population distribution $m_{\rm JFC}$ is given by

$$m_{\rm JFC}(a,e,i,H)\,{\rm d}a\,{\rm d}e\,{\rm d}i\,{\rm d}H = B(a,e,i,H)\times M_{\rm JFC}(a,e,i,H)\,{\rm d}a\,{\rm d}e\,{\rm d}i\,{\rm d}H, \quad (4)$$

where $B(a,e,i,H)$ represents the observational selection effects (bias) of the survey(s) contributing to the observed population as a function of the object's H, semimajor axis (a), eccentricity (e), and inclination (i). $B(a,e,i,H)$ can be thought of as the probability that an object with (a,e,i,H) has been detected. $M_{\rm JFC}(a,e,i,H)\,{\rm d}a\,{\rm d}e\,{\rm d}i\,{\rm d}H$ represents the actual number of JFCs with orbit elements and H in the ranges $a \to a+{\rm d}a$, $e \to e+{\rm d}e$, $i \to i+{\rm d}i$, and $H \to H+{\rm d}H$.

We assume that the H-distribution of the JFCs is independent of their orbital distribution so that we can write

$$M_{\rm JFC}(a,e,i,H) = \tilde{f}_{\rm JFC}(a,e,i)\times C_0 \times 10^{\alpha(H-H_0)}, \quad (5)$$

where $\tilde{f}_{\rm JFC}(a,e,i)\,{\rm d}a\,{\rm d}e\,{\rm d}i$ is the fraction of the JFC population with orbit elements $(a,e,i) \to (a+{\rm d}a, e+{\rm d}e, i+{\rm d}i)$ and $C_0 = \alpha N_0 \ln(10)$, where N_0 is the number of JFCs with $H < H_0$.

Our goal is to determine the slope (α) of the H-distribution of dormant JFCs. As we will see below (Section 2.1), α is the only free parameter in our model distribution $M_{\rm JFC}$. Thus, we can determine its value by looking for the best 4-dimensional fit in the (a,e,i,H)-space between the model distribution $B \times M_{\rm JFC}$ and the observed distribution $m_{\rm JFC}$.

To do so, we first need to select the NEOs that are most likely to be dormant JFCs in order to define the $m_{\rm JFC}$ distribution (Section 2.1), then build the distribution model $M_{\rm JFC}$ in a consistent way (Section 2.2), and evaluate the bias function B (Section 2.3). The fitting procedure is explained in Section 2.4.

2.1. Selection of dormant JFC candidates

We started from a list of 2677 known NEOs provided by the Harvard-Smithsonian's MPC data archive on March 5, 2004. These NEOs are *not* known to be comets, i.e., none of them are known to have ever displayed evidence of cometary activity. Thus, if some of them are comet nuclei, they are either dormant, extinct, or outgassing at an undetectable level. Their absolute magnitudes therefore correspond to the brightness of their bare nucleus.

To identify potential dormant JFCs among the NEOs, we used the Bottke et al. (2002a) model. Given a set of values for a, e, and i, the model provides the probability, $P_{\rm JFC}(a,e,i)$, that the corresponding object is a JFC. This is possible because the characteristic orbital distributions for NEOs of JFC origin and of asteroidal origin are distinct even though they partially overlap. Fig. 1 shows the orbit distribution for NEOs of non-JFC and JFC provenance according to the Bottke et al. (2002a) model. It is important to keep in mind that these figures show the 3-dimensional (a,e,i) space collapsed into two dimensions and, therefore, that the amount of overlap between the orbit distributions is exaggerated. The orbit distributions in Fig. 1 embody all our knowledge of the source region for the NEOs as a function of their orbit elements.

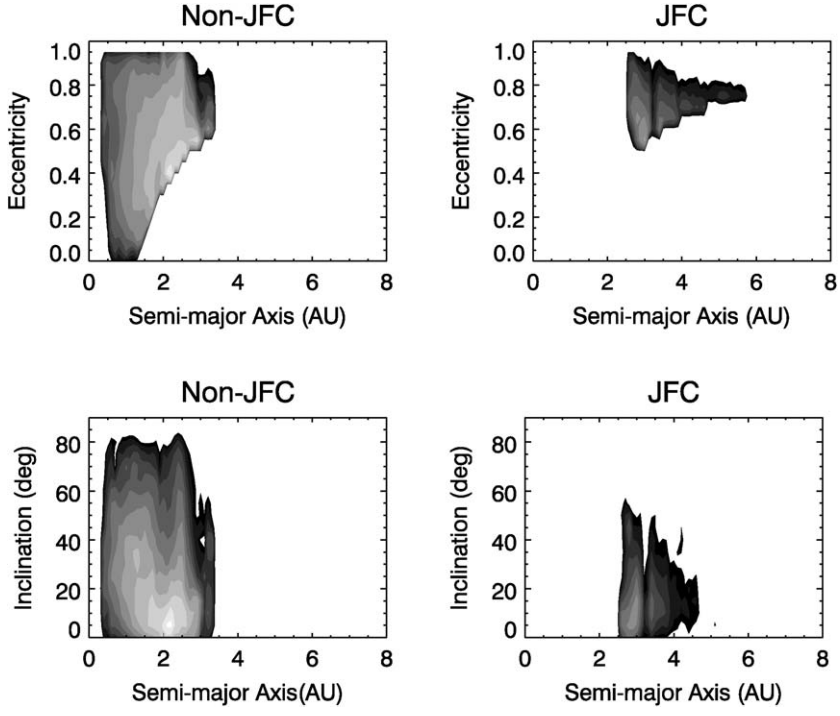

Fig. 1. (Left) Orbit distribution for all non-JFC NEOs according to the Bottke et al. (2002a) model. (Right) Orbit distribution for NEOs of JFC origin according to the same model.

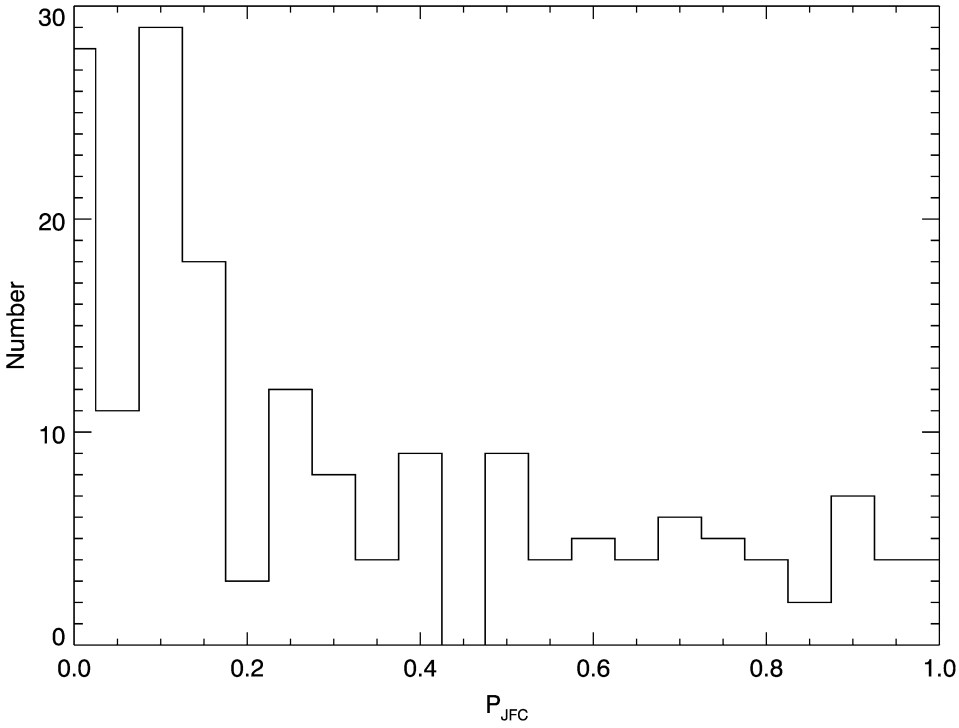

Fig. 2. Distribution of the probability that known NEOs derive from the JFC source region according to the Bottke et al. (2002a) model. Only objects with $P_{\rm JFC} > 0.01$ are shown.

The condition $P_{\rm JFC}(a, e, i) > 0$ selects 1657 objects. Nevertheless, for most of these objects $P_{\rm JFC}$ is very small (<0.01), so they are likely to be asteroids even if a JFC origin cannot be ruled out. Fig. 2 shows the distribution of $P_{\rm JFC}$ for those objects with $P_{\rm JFC} > 0.01$ and illustrates that restricting the NEO sample to objects with increasingly larger $P_{\rm JFC}$ reduces the fraction of asteroid interlopers. On the other hand, it also reduces the total number of objects and eventually runs the data into the noise. Thus, there is a trade-off on the choice of the threshold value of $P_{\rm JFC}$, hereafter denoted by $P_{\rm cutoff}$, used to select our sample of candidate dormant JFCs.

We set $P_{\rm cutoff}$ to the value that maximizes the signal-to-noise ratio carried by the NEOs of JFC origin. The signal-to-noise ratio for a specific $P_{\rm cutoff}$ is given by

$$\frac{S}{N}(P_{\rm cutoff}) = \frac{\text{Signal}}{\sqrt{\text{Signal} + \text{Background}}} \tag{6}$$

$$= \frac{\sum_i^{P>P_{\rm cutoff}} P_i}{\sqrt{\sum_i^{P>P_{\rm cutoff}} P_i + \sum_i^{P>P_{\rm cutoff}} (1 - P_i)}}, \tag{7}$$

$$\frac{S}{N}(P_{\rm cutoff}) = \frac{\sum_i^{P>P_{\rm cutoff}} P_i}{\sqrt{\sum_i^{P>P_{\rm cutoff}} 1}}, \tag{8}$$

where P_i is the JFC probability for object i. Because the S/N function is not smooth we fit a second-order polynomial to the curve. The shape of this function is shown in Fig. 3 where it is clear that a maximum $S/N \sim 5.7$ is achieved at $P_{\rm cutoff} = 0.37$. There were a total of 67 NEOs with $P_{\rm JFC} \geqslant 37\%$. We then confirmed that all but one of them (2004 CB) had never displayed any cometary activity (http://www.ifa.hawaii.edu/~yan/cometlist.html). That object was removed from the data set leaving us with 66 candidate dormant JFC nuclei.

The bias calculation (Section 2.3) proved to be computationally intensive so we chose to eliminate five of the JFC candidates with outlying orbit elements. This allowed us to restrict the range of (a, e, i, H) over which we needed to determine the bias to 2.6 AU $\leqslant a <$ 3.8 AU, $0.55 \leqslant e < 0.95$, $0° \leqslant i < 55°$, $14.0 \leqslant H < 22.5$.

Our final sample of 61 NEOs are listed in Table 1 while Fig. 4 shows the (a, e, i, H) distributions of these objects. There are many new unnumbered asteroids listed in the table and their orbital elements are usually not as accurately known as the numbered asteroids. This is of no consequence to our analysis because the binning we will use in (a, e, i) is much larger than the typical error on unnumbered asteroid orbital elements and because $P_{\rm JFC}$ usually varies slowly and smoothly across adjacent bins.

Of course, it is disturbing to base our selection of dormant JFC candidates on a model. If the Bottke et al. (2002a) model provides a function, $P_{\rm JFC}(a, e, i)$, that is inaccurate our selected candidates might not be optimal. To strengthen the validity of our assumptions we will show (Section 3.1) that our selected distribution, $m_{\rm JFC}$, is matched by our JFC model distribution, $B \times M_{\rm JFC}$, at a satisfactory statistical level. A positive result implies that, irrespective of how we selected the observed population, the latter is likely to be dominantly of JFC origin. In Section 3.2 we will also discuss the dependence of the resulting value of α (the exponent of the H-distribution) on the assumed value of $P_{\rm cutoff}$.

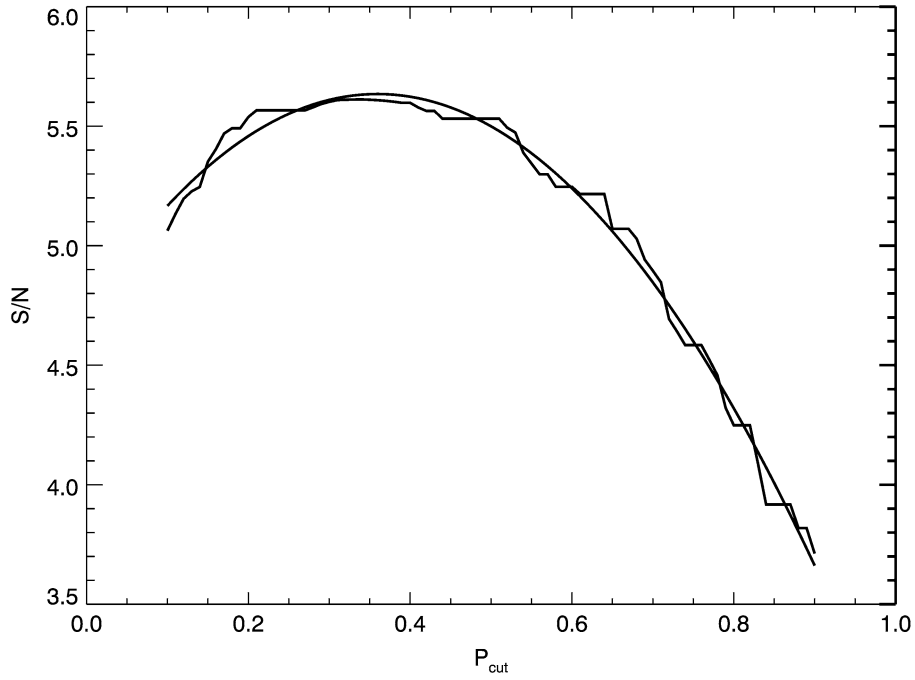

Fig. 3. The variation of the S/N, and the second-order polynomial fit to that curve, as a function of the cutoff on the probability that the objects are NEOs derived from the JFC source region. The maximum S/N occurs at $P_{\rm cutoff} = 0.37$.

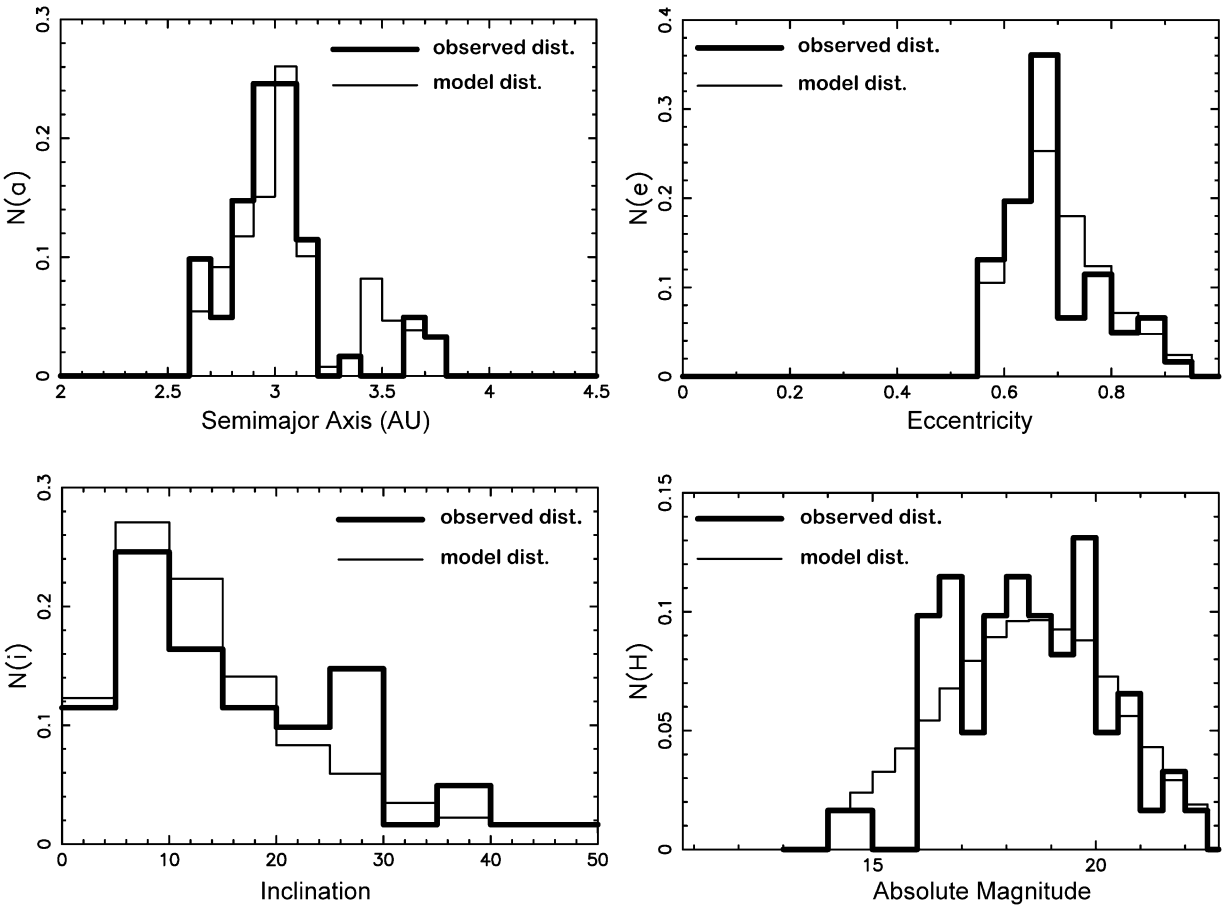

Fig. 4. Bold histograms: the semimajor axis, eccentricity, inclination, and absolute magnitude distributions for dormant JFC candidates among the NEO population. Light histograms: the same distributions for our model $B \times M_{\rm JFC}$ obtained for the value of α leading to the best quantitative match.

Table 1
Dormant JFC candidates selected from known NEOs

Designation	a	e	i	H	$P_{\rm JFC}$
2004 BZ74	3.05	0.893	16.6	18.7	0.98
2003 YS1	3.10	0.847	25.1	19.7	0.42
2003 WY25	3.08	0.675	5.9	21.1	0.88
2003 WR25	3.35	0.710	9.0	19.6	0.94
2003 UO12	2.74	0.700	45.1	15.4	0.54
2003 HP32	2.69	0.779	3.4	19.7	0.51
2002 XE84	2.82	0.663	28.9	20.7	0.44
2002 UO3	2.96	0.802	24.1	17.8	0.91
2002 MT3	2.81	0.690	6.5	19.9	0.64
2002 KG4	2.94	0.663	27.6	20.9	0.78
2002 JB9	2.72	0.785	46.7	16.0	0.55
2002 GZ8	2.79	0.653	5.3	18.4	0.39
2002 GJ8	2.96	0.828	5.3	19.3	0.98
2002 FC	2.83	0.661	6.8	19.0	0.64
2002 EX12	2.60	0.767	11.3	16.1	0.55
2002 CX58	2.80	0.659	2.5	22.2	0.54
2001 YK4	2.65	0.778	4.6	18.5	0.51
2001 XP1	2.90	0.751	39.3	17.8	0.78
2001 QN142	3.09	0.686	10.2	21.8	0.90
2001 ME1	2.65	0.865	5.8	16.9	0.41
2000 YG29	3.17	0.695	18.9	18.8	0.78
2000 WL10	3.16	0.714	10.2	18.0	0.93
2000 PG3	2.83	0.858	20.5	16.2	0.93
2000 KE41	3.00	0.865	50.4	17.4	0.82
2000 DN1	2.88	0.670	7.8	19.7	0.64
1999 UZ5	2.64	0.799	10.4	21.8	0.55
1999 RD32	2.64	0.771	6.8	16.6	0.53
1998 SY14	2.85	0.665	3.5	20.6	0.54
1998 FR11	2.79	0.713	6.6	16.4	0.65
1984 QY1	2.97	0.917	15.5	14.0	0.96
1986 JK	2.85	0.665	2.0	18.3	0.54
2003 SD201	3.03	0.640	20.9	17.9	0.71
2003 RM	2.91	0.604	10.9	20.1	0.43
2003 LO6	2.91	0.576	34.6	16.8	0.69
2003 AC1	3.14	0.653	23.5	20.7	0.57
2002 WW17	3.02	0.654	18.4	17.6	0.83
2002 VT94	3.09	0.587	25.1	19.7	0.90
2002 UN	3.01	0.609	26.2	17.3	0.94
2002 RC118	2.95	0.565	28.0	16.8	0.72
2002 RN38	3.80	0.675	3.8	17.3	1.00
2002 AO7	2.94	0.626	14.9	18.2	0.43
2002 AR4	3.00	0.622	8.3	20.0	0.80
2001 XQ	3.64	0.713	29.0	19.5	1.00
2001 UU92	3.17	0.669	5.4	20.1	0.68
2001 TB45	3.00	0.576	25.1	19.0	0.72
2001 SK169	3.01	0.568	20.2	17.6	0.67
2001 AO2	3.07	0.609	19.9	18.3	0.60
2000 LF6	2.91	0.611	14.8	19.9	0.43
2000 EB107	3.03	0.585	25.3	16.9	0.90
1999 VX15	3.01	0.600	12.3	18.8	0.72
1999 LT1	2.98	0.657	42.6	17.6	0.74
1999 DB2	3.00	0.620	11.6	19.1	0.72
1998 SE35	3.01	0.593	14.8	19.2	0.41
1998 HN3	3.12	0.618	9.2	18.4	0.55
1998 GL10	3.18	0.668	8.7	18.5	0.68
1997 SE5	3.73	0.666	2.6	14.8	1.00
1992 UB	3.07	0.581	15.9	16.3	0.42
1982 YA	3.66	0.700	35.3	16.5	0.97
1982 YA	3.63	0.697	35.0	18.1	0.83
1998 MX5	2.98	0.612	9.7	18.5	0.58
1994 LW	3.19	0.617	22.4	16.9	0.71

2.2. Model for NEOs of JFC provenance

Following Bottke et al. (2002a), we used the numerical simulations by Levison and Duncan (1997) as our model for the orbital distribution of JFCs. These authors simulated the dynamical evolution of 2200 test bodies initially in the trans-neptunian scattered disk. The orbits of these bodies were tracked until they entered a major sink or until the integration time elapsed. Particles reaching $a < 2.5$ AU orbits were cloned 9 times to increase statistics in this zone.

Bottke et al. (2002a) kept track of the amount of time spent by each object within cells of a 3-dimensional grid in (a, e, i) orbital space, covering the NEO region ($q = a(1-e) < 1.3$ AU) with a resolution of (0.1 AU, 0.05, 5°). This "residence-time distribution" represents the steady-state relative distribution of JFCs in NEO space as shown in Fig. 7 of Bottke et al. (2002a).

Since we selected the dormant JFC candidates as the NEOs with $P_{\rm JFC} > P_{\rm cutoff}$, for internal consistency we need to restrict $f_{\rm JFC}(a, e, i)$ to those (a, e, i)-bins over which $P_{\rm JFC}(a, e, i) > P_{\rm cutoff}$ and set the function equal to zero elsewhere. Thus, the function $\tilde{f}_{\rm JFC}(a, e, i)$ introduced in (5) is re-defined as

$$f'_{\rm JFC}(a, e, i) = \tilde{f}_{\rm JFC}(a, e, i) \quad \text{if } P_{\rm JFC}(a, e, i) \geqslant P_{\rm cutoff}, \tag{9}$$

$$f'_{\rm JFC}(a, e, i) = 0 \quad \text{if } P_{\rm JFC}(a, e, i) < P_{\rm cutoff}, \tag{10}$$

and then $f'_{\rm JFC}$ is normalized to produce $f_{\rm JFC}$. The function $f_{\rm JFC}(a, e, i)$ can be regarded as a probability function for the orbital distribution of JFCs over the restricted (a, e, i) region.

It is important to note that in building $f_{\rm JFC}(a, e, i)$ there is only a single free parameter: $P_{\rm cutoff}$. This threshold only determines the range in the (a, e, i) orbital element space over which the model is normalized and used. Furthermore, we will show below that our result is only weakly dependent on the choice of $P_{\rm cutoff}$ and this is an effect of altering the data rather then altering $f_{\rm JFC}(a, e, i)$.

We assume that the H-distribution is independent of (a, e, i) and can be expressed in the simple form of Eq. (1). The final JFC distribution model $M_{\rm JFC}(a, e, i, H)$ is then the product of $f_{\rm JFC}$ with the H-distribution as shown in Eq. (5). The exponent α defining the H-distribution is the only free parameter of our model that we will fit to the observations. Note that the individual $P_{\rm JFC}$ are independent of H since they depend only on the orbital elements in Bottke et al.'s (2002a) residence-time distributions.

2.3. Bias determination

Many factors determine whether an object will be discovered by a survey: limiting magnitude, seeing, detector efficiency, weather conditions, field of view, sky coverage, etc. The overall probability that an object with (a, e, i, H) will be discovered is virtually impossible to calculate analytically except for the most trivial surveys. Instead, the bias can be determined through a Monte Carlo simulation of the detector's performance that takes into account important factors determining the observational

selection effects (Jedicke et al., 2002). The calculation is complicated by the fact that all the determining factors may vary from field to field even within a single survey.

Our data sample (Section 2.1) is comprised of NEOs discovered by 13 different observatories: Spacewatch, LINEAR, LONEOS, Catalina Sky Survey, NEAT, CINEOS, AMOS, Palomar, Siding Spring Observatory, Dynic Astronomical Observatory, Lomnicky Stit, Berne-Zimmerwald, and Haute Provence. It would be preferable to generate the bias function using detailed performance criteria from each survey but this information is difficult or impossible to obtain. We could have chosen to use only objects discovered by a single well-characterized survey, but this would have compromised the number statistics of dormant JFCs within the NEO population available for the study and decreased the S/N of our result.

Consequently, we chose to follow a different strategy. Jedicke et al. (2003) developed a software simulator to imitate, within a single synthetic survey, the cumulative performance of all real surveys that have contributed to discovering NEOs. The simulator incorporated a number of characteristics typical of asteroid and comet surveys: field locations, limiting magnitude, minimum detectable rate of motion, minimum galactic latitude, and detector efficiency. It passed a number of tests and detailed comparisons with the performance of individual well-characterized surveys as discussed in Jedicke et al. (2003). Essentially, starting from the Bottke et al. (2002a) model it is able to recover the observed orbital and H-distribution of real NEOs. The simulator has been used by Jedicke et al. (2003) to correctly predict the fall-off of the NEO discovery rate by the LINEAR survey that has been observed over the past two years. Moreover, it has been used by Levison et al. (2002) to estimate the fraction of dormant LPCs that surveys should have detected and, consequently, to determine that most LPCs disrupt rather than become extinct or dormant.

We have used the Jedicke et al. (2003) simulator to compute the bias function $B(a, e, i, H)$ in the following manner. We generated a large number of synthetic objects $G(a, e, i, H)$ and then determined which were discovered by the simulator, $D(a, e, i, H)$. The simulated survey bias is then simply

$$B(a, e, i, H) = \frac{D(a, e, i, H)}{G(a, e, i, H)}, \tag{11}$$

with an uncertainty of

$$\sigma_B(a, e, i, H) = \sqrt{\frac{B(1 - B)}{D}}. \tag{12}$$

We determined the bias for the candidate dormant JFC nuclei specified in Section 2.1 ($2.6\ \text{AU} \leqslant a < 3.8\ \text{AU}$, $0.55 \leqslant e < 0.95$, $0° \leqslant i < 55°$, $14.0 \leqslant H < 22.5$) using bins of size (0.1 AU, 0.05, 5°, 0.5), respectively. There were a total of 639,360 bins in the calculation. The synthetic NEO population, $G(a, e, i, H)$, was the sum of three separately generated sets of objects:

- 10^6 objects distributed evenly among all the bins to ensure that $G(a, e, i, H) \neq 0$ for each a, e, i, H. This is important to ensure that the bias function is defined in every cell of the model.
- 10^6 objects distributed evenly in (a, e, i), but proportional to $10^{0.5H}$ in H. This was done in order to generate more objects in bins for which the error on the bias determination will be large due to small D (see Eq. (12)). Generating more objects in these bins means that the simulator will also find more of them.
- 10^5 objects generated in *each* of the bins corresponding to the 61 NEOs in our sample (see Table 1). For example, 100,000 objects were generated in the bin occupied by 2004 BZ74 with $3.0 \leqslant a < 3.1$, $0.85\ \text{AU} \leqslant e < 0.9\ \text{AU}$, $15.0° \leqslant i < 20.0°$, $18.5 \leqslant H < 19$. This is important to ensure that we have a good measure of the bias in each bin incorporated in the numerator of the ML method (Eq. (15)).

For all three sets, the orbital angles: mean anomaly, longitude of node, and longitude of perihelion were assumed to be randomly distributed. The final synthetic population contained over 8 million objects that were then "surveyed" by the simulator. The simulation was run for 2393 synthetic days (~6.6 y), defined by the time required by the simulator to discover 694 objects (the number of known NEOs as of March 5, 2004, the date of the catalogue from which the list of dormant JFC candidates was extracted) out of the synthetic population of NEOs in the Bottke et al. (2002a) model.

Representative slices through the bias function, $B(a, e, i, H)$, are provided in Fig. 5 showing a smooth variation of the discovery probability as a function of the orbital elements and H. A comparison of Fig. 5A with Fig. 5B shows that as the objects become smaller they become more difficult to detect. The effect of inclination on the observational bias is not so strong (compare the progression in Figs. 5A, 5C, and 5D) due to the fact that modern NEO surveys cover much of the sky to high ecliptic latitudes.

2.4. Maximum-likelihood determination of the slope

In this section we lay the mathematical groundwork that is used in the final calculation of the slope, α. The maximum-likelihood (ML) technique is our method of choice, as it is a powerful tool for fitting a model to an unbinned data distribution (Lyons, 1986). The ML method determines the parameters of the fit that maximizes the probability that the model matches the data.

We illustrate the ML method for a function $F(\vec{x}, \alpha)$, where F represents our biased model $B \times M_{\text{JFC}}$, the vector $\vec{x}$ represents the 4-dimensional coordinates (a, e, i, H), and α is the free parameter. First, we calculate the normalization factor $N(\alpha) = \int F \, \mathrm{d}\vec{x}$ over the allowed domain of $\vec{x}$. Thus, $F(\vec{x}', \alpha')/N(\alpha')$ is proportional to the probability that an event with $\vec{x} = \vec{x}'$ will occur when $\alpha = \alpha'$. If there are n events (observations) with $\vec{x} = \vec{x}_i$ $(i = 1, n)$, then the probability of obtaining

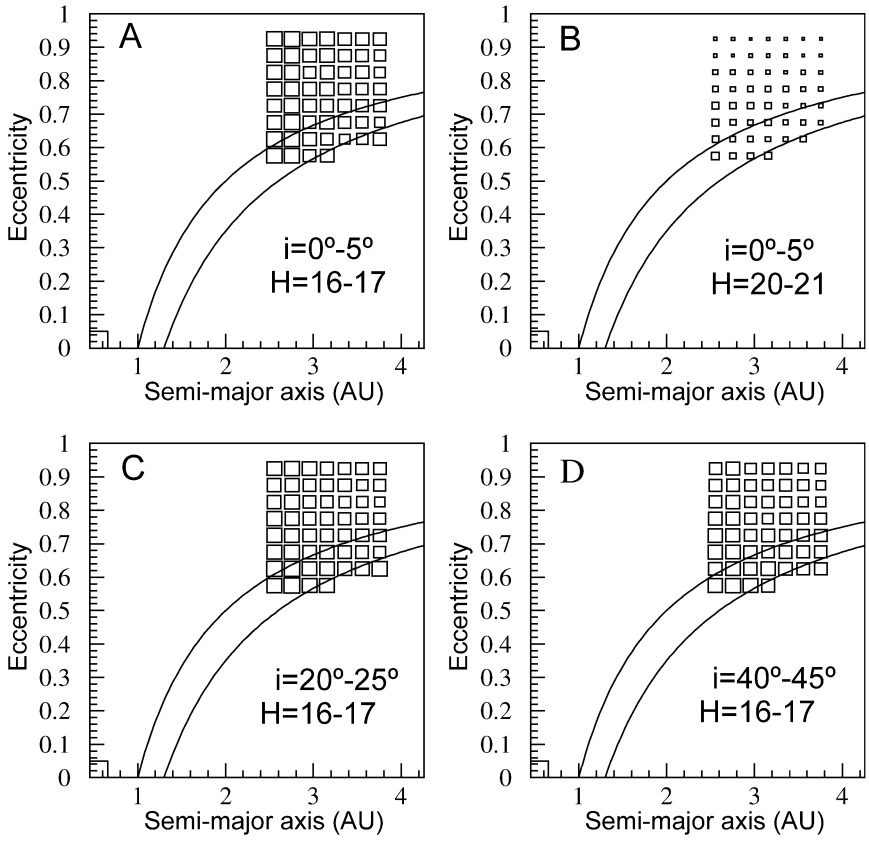

Fig. 5. Four 2-dimensional (i, H) slices through $B(a, e, i, H)$. The ranges of i and H are shown on each of the four figures. $B(a, e, i, H)$ was calculated only in the orbital element range (see Section 2.1) in which the JFCs used in this study are found. The size of each box is proportional to the probability (bias) of discovering an object with orbit elements and absolute magnitude within the box. All objects above the lower solid curve are NEOs (with perihelion <1.3 AU) while all objects above the upper solid curve are Earth crossing (with perihelion <1.0 AU).

those n events with the fit parameter α is proportional to

$$\mathcal{L}(\alpha) = \prod_{i=1}^{n} \frac{F(\vec{x}_i, \alpha)}{N(\alpha)} \tag{13}$$

$$= \prod_{i=1}^{n} \frac{F(\vec{x}_i, \alpha)}{\int F(\vec{x}, \alpha)\, \mathrm{d}\vec{x}}. \tag{14}$$

Maximizing $\mathcal{L}$ provides the most probable value of α. The second line of this equation is important because it emphasizes the fact that the denominator relies on a normalization over the entire range of F and is a function of the fit parameter (α) while the numerator depends on the n values at the specific $\vec{x}_i$.

For the purpose of maximizing Eq. (13) it is beneficial to take its logarithm to convert the product into a sum. Maximizing the logarithm of a function is equivalent to maximizing the function itself. The function then becomes

$$l = \ln(\mathcal{L}) = \sum_{i=1}^{n} \ln\left[\frac{F(\vec{x}_i, \alpha)}{N(\alpha)}\right]. \tag{15}$$

The value of α when l is at its maximum $(l_{\max})$ is the best fit of the model to the data. In the ML method, the statistical error on the most probable result is found by obtaining the values of α at $l_{\max} - 1/2$ on both the positive and negative sides of α. The errors are then $\sigma_+ = \alpha(l_{\max} - 1/2)_+ - \alpha(l_{\max})$ and $\sigma_- = \alpha(l_{\max}) - \alpha(l_{\max} - 1/2)_-$, where the $+$ and $-$ designate larger and smaller values of α, respectively (Lyons, 1986).

3. Model results

Using the procedure described in the previous section and illustrated in Fig. 6, we find that the best agreement between model and observation is achieved with an exponent of the H-distribution for dormant JFCs in NEO space of

$$\alpha = 0.30 \pm 0.03\ (\text{stat}) \pm 0.05\ (\text{sys}). \tag{16}$$

The first quoted error is statistical only while the second is an estimate of the systematic (model-dependent) error introduced by our technique. The determination of the systematic error is discussed briefly in Section 3.3.

Before we discuss the implications of this result we need to verify that our result is meaningful. The fact that we have found a best fit does not imply that the fit is good. This would be the case, for instance, if our selected sample of dormant JFC candidates contained too many asteroids whose orbital distribution cannot be matched with that of JFCs. Alternative reasons for a bad fit could be that our orbital distribution model for JFCs is flawed (for instance, the effects of terrestrial planets or of non-gravitational forces—not included in the integrations by Levison and Duncan, 1997—might not be negligible), or that

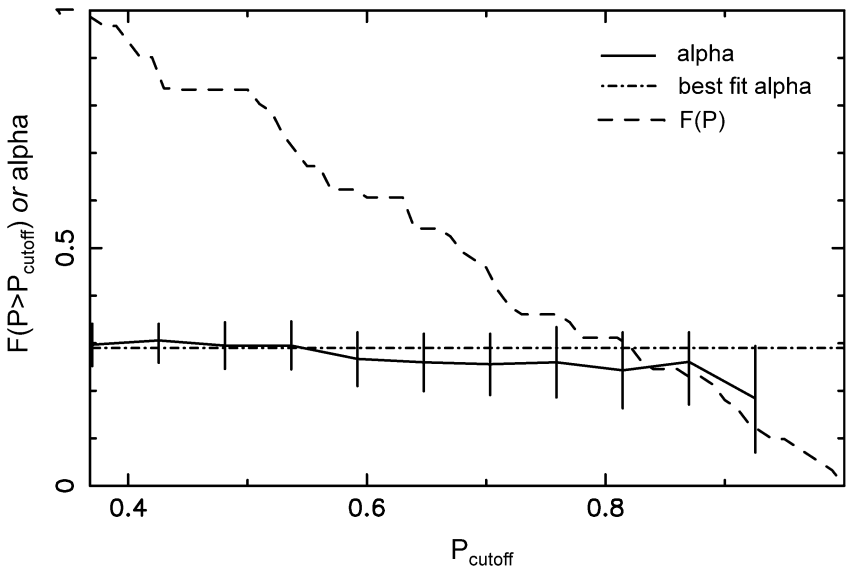

Fig. 6. Dashed line: the fraction of our original 61 NEO sample that remains selected if $P_{\rm cutoff}$ is increased beyond our preferred value of 0.37. Solid line: the value of α obtained by best fit of the model to the restricted NEO sample of dormant JFC candidates as a function of $P_{\rm cutoff}$. The horizontal dash-dotted line indicates our preferred value of $\alpha = 0.30$.

our evaluation of the biases is unrealistic. Conversely, if we can show that the fit is good, this would be a strong indication that all our assumptions for the selection of the data, construction of the model, and evaluation of the biases, are reasonable, and that our best fit α is representative of the real SFD of dormant JFCs.

Fig. 4 shows our best fit model distribution, $B \times M_{\rm JFC}$, collapsed into 1-dimensional histograms with respect to a, e, i, and H. A visual comparison with the observed distributions in each parameter suggests that our model reproduces reality well. However, a qualitative visual agreement is a necessary but not sufficient condition for a quantitative match between the model and real 4-dimensional (a, e, i, H) distributions. Testing the actual match between the distributions requires a numerical analysis that we develop in the next section.

3.1. Quantifying the statistical agreement between model and observations

In order to quantitatively estimate the statistical agreement between the model and the observations we have followed the procedure implemented by Bottke et al. (2002a). From the best fit model ($B \times M_{\rm JFC}$, with $M_{\rm JFC}$ obtained with the best fit value of α in the H-distribution), we have randomly generated 20,000 synthetic sets of 61 objects each. Remember that 61 is the number of dormant JFCs candidates that we selected in (Section 2.1), so that each of the synthetic datasets that we generated has the same number of data points as the actual data.

By construction, the synthetic datasets 'perfectly' match the model. We then computed the likelihood value, l, using (15) for each of the generated 20,000 synthetic datasets. The *distribution* of l gives the probability that a likelihood l' is obtained from a dataset that is in perfect agreement with the model. We found that in 42% of the synthetic data sets the likelihood values were *lower* than the likelihood obtained for the actual data. We conclude that our best fit model has a 42% probability of being in statistical agreement with the data. In other words, our model fits the data to within better than 1 σ and that we have reproduced the observed distribution of dormant JFC candidates. In light of this success, all our assumptions in selecting JFC candidates and in building the model appear justified.

3.2. Dependence of the best fit result on the choice of $P_{\rm cut}$

Despite the good results illustrated above it is still legitimate to ask how our result on the best fit value of α would change if we chose a more stringent value of $P_{\rm cutoff}$. As $P_{\rm cutoff}$ is increased we reduce the contamination of the dormant JFC candidates by asteroids, but reduce the total number of objects in our sample with a concomitant increase in the statistical error on the measurement of the slope. The dashed line in Fig. 6 shows the fraction of our original 61 object sample that remains as $P_{\rm cutoff}$ is increased beyond our preferred choice of 0.37. The solid curve shows the value of $\alpha \pm \delta\alpha$ determined by the best fit to the model for the restricted sample.

We see that the calculated value of α is consistent with being constant and equal to our nominal value over the entire range of $P_{\rm cutoff}$ values. On the other hand, there is a small and systematic decrease in α with $P_{\rm cutoff}$ for $P_{\rm cutoff} \gtrsim 0.6$. This might be interpreted in two ways. A first possibility is that with $P_{\rm cutoff} = 0.37$ we have some asteroid contamination in our data sample (according to the Bottke et al. (2002a) model about 1/3 of our selected objects should be asteroids). So, the value of α that we determine is a weighted average between the slope characterizing NEOs of asteroidal origin ($\alpha = 0.35$ according to Bottke et al., 2002a) and the actual α of dormant JFCs. By increasing $P_{\rm cutoff}$ we reduce the asteroid contamination and the genuine value of α for the JFCs is exposed. The second possibility is that α changes simply because we are fitting a smaller dataset,

but the results are still statistically consistent with $\alpha = 0.30$ as shown in Fig. 6. The fact that our choice of $P_{\rm cutoff}$ maximizes the signal/noise ratio of the JFC sample (Section 2.1), and that the corresponding data set is well matched by our model, makes us confident that $\alpha \sim 0.30$ is a measure of the real slope of the H-distribution of dormant JFCs.

3.3. Systematic errors

The error bars on the best fit values of α, illustrated in Fig. 6, represent the statistical errors given by the ML fitting method (Section 2.4). However, the technique itself is model-dependent and introduces systematic errors into our α determination. As always, the systematic error should be quantified wherever possible.

There are a number of model-dependent sources of error in our slope determination. Our use of the nominal Bottke et al. (2002a) model for the JFC probability as a function of (a, e, i) could be a source of systematic error. If the actual dynamical distribution or contributions of the source populations going into that model are different from the assumption it would affect our slope determination. We consider it unlikely that the dynamical distribution of the source populations could be much different from that used in the Bottke et al. (2002a) analysis because it used high-statistics and a dynamical integrator of good pedigree. On the other hand, the contribution from each of the 5 source regions (or even the inclusion of other possible sources) was determined from a fit to the model for a small number of data points. The relative contribution from each source could be different from the nominal model. Recent, as-yet-unpublished work (Bottke, personal communication) suggests that the inclusion of 10× more data using the results of the LINEAR survey have little effect on the fraction of the NEO population deriving from each source population.

To estimate this systematic effect, let $f_{\rm JFC}$ represent the fraction of the NEO population from the JFC source region and $p_{\rm JFC}(a, e, i, H)$ be the dynamical probability that a JFC will appear in the bin near (a, e, i, H). Similarly, let f_x represent the fraction of the NEO population from all other sources and $p_x(a, e, i, H)$ be the dynamical probability that an object from any other source will appear in the same bin. Then the probability that an object is a JFC in that bin is simply

$$P_{\rm JFC} = \frac{f_{\rm JFC}\, p_{\rm JFC}}{f_{\rm JFC}\, p_{\rm JFC} + f_x\, p_x}. \tag{17}$$

Recognizing that $f_{\rm JFC} = 1 - f_x$ and differentiating with respect to the JFC fraction ($f_{\rm JFC}$) we find that

$$\mathrm{d}P_{\rm JFC} = \left[p_{\rm JFC} - p_{\rm JFC}^2 \left(1 - \frac{p_x}{p_{\rm JFC}} \right) \right] \frac{\mathrm{d}f_{\rm JFC}}{f_{\rm JFC}}, \tag{18}$$

$$\mathrm{d}P_{\rm JFC} \approx p_{\rm JFC}(1 - p_{\rm JFC}) \frac{\mathrm{d}f_{\rm JFC}}{f_{\rm JFC}}, \tag{19}$$

where we have made the approximation that $p_x / p_{\rm JFC} \ll 1$ since we are expressly working with a region in (a, e, i)-space that has a high-probability of containing objects of JFC provenance. Bottke et al. (2002a) calculated that $f_{\rm JFC} = 0.06 \pm 0.04$ and we used $P_{\rm JFC} = 0.37$ so that we expect the effect of an inaccurate determination for the fraction of the NEO population that are JFCs to be on the order of $\mathrm{d}P_{\rm JFC} \sim 0.15$. Fig. 6 shows that the calculated value for the slope is relatively insensitive to changes in $P_{\rm JFC}$ of this magnitude so that we consider this to be a negligible source of systematic error.

Fig. 6 further explores the systematic error introduced by our selection of $P_{\rm cutoff}$. In that figure we vary that value over the range from 0.37 to 0.7 and obtain best fit values for α ranging from 0.310 to 0.256. We associate half this difference, or 0.027, with the systematic error introduced due to the data selection process.

Another source of systematic error is the bias estimate. As we explained in Section 2.3, to compute the bias function we performed a survey simulation for a large population of realistic synthetic NEOs (Bottke et al., 2002a). The parameters of the survey simulator were empirically 'tuned' to provide a distribution of 'discovered' objects that mimicked the known distribution (Jedicke et al., 2003). Nevertheless, some uncertainty remains in the survey simulator's parameters. The most important one is the limiting magnitude of the simulated survey. In Section 2.3 we used $V_{\rm lim} = 20.5$ but a choice of $V_{\rm lim}$ 0.5 magnitudes fainter or brighter would give a similarly good reconstruction of the observed NEO population. Thus, we computed two additional bias functions by running the simulator with $V_{\rm lim} = 20.0$ and $V_{\rm lim} = 21.0$. The number of virtual days over which the simulation was run was also changed so that the total number of discovered synthetic NEOs remained equal to the actual number of NEOs found by real surveys. Then, using these new bias functions, we repeated the fitting procedure detailed in this paper and found that the best fit value of α changed by ± 0.04 with respect to our nominal value of 0.30.

Thus, we estimate that the magnitude of the systematic error on the best fit slope for the H-distribution is the quadratic sum of the two values given above or 0.05 as stated in Eq. (16).

4. Discussion

Using our best fit model, we can estimate the total number of dormant JFCs. For this purpose, we first need to evaluate the weighted mean bias $\bar{B}$, defined as

$$\bar{B} = \sum_{(a,e,i)} \sum_{14<H<22.5} B(a, e, i, H)\, M_{\rm JFC}(a, e, i, H), \tag{20}$$

where the first sum is computed over all the (a, e, i) cells for which $P_{\rm JFC} \geqslant P_{\rm cutoff}$, $M_{\rm JFC}(a, e, i, H)$ is our best fit normalized model (where $\sum_{(a,e,i)} \sum_{14<H<22.5} M_{\rm JFC}(a, e, i, H) = 1$), and we only sum over bins for which $B(a, e, i, H) \neq 0$. We find $\bar{B} = 8.22 \times 10^{-3}$.

Thus, the 61 dormant JFCs discovered over the same (a, e, i, H) range imply a total population of ∼1400 objects with $H < 22.5$. Given our best fit value of α, the population of dormant JFCs with $H < 18$ is $1400 \times 10^{[-0.30\times(22.5-18)]} \sim 63$. However, this is the number within the restricted region where $P_{\rm JFC}(a, e, i) > 0.37$ rather than the total number of JFCs in the entire NEO region. From the orbital distribution model that we have adopted (Section 2.2), we compute that the total number

of JFCs with $a < 7.4$ AU and $q < 1.3$ AU (i.e., JFCs in the NEO region) should be larger by a factor of ∼1.2, implying ∼75 objects with $H < 18$. There are about 25 known objects in this size range in our data sample implying a completion rate of about 1/3 for dormant JFCs with $H < 18$. This may be compared to the current completion of about 70% for all NEOs with $H < 18$. The reduced completion rate for the dormant JFC NEOs is easily understood as an observational selection effect due to their large eccentricity and correspondingly larger heliocentric distance.

This number is in good agreement with that of 61 ± 43 determined by Bottke et al. (2002a) and we stress that our result is independent of their calculation. The only thing that the present work has in common with the earlier work is the orbital distribution model for JFCs. The bias function and the data used to fit the model are different. The use of $P_{\rm JFC}$ from Bottke et al. (2002a) in the selection of our data is only incidental as discussed in Section 2.2. Thus, the agreement between the two results strengthens both models.

Fernández et al. (1999) claim that there are 30^{+10}_{-5} active JFCs with $H < 18$ and $q < 1.3$ AU while Levison and Duncan (1997) suggest that for each active comet there should be 3.5 faded comets (ranging from a minimum of 2.0 to a maximum of 6.7). Thus, assuming that all faded comets are dormant, we estimate that the total number of dormant JFCs with $H < 18$ and $q < 1.3$ AU is $30 \times 3.5 = 105$, with a possible range from 50 to 270. Our estimate of the actual number of dormant JFCs falls at the lower end of this range but not too far from the nominal value. We conclude, as in Bottke et al. (2002a), that a substantial fraction of JFCs become dormant when they fade. Unlike in the LPC and HTC cases (for which only ∼1% of faded comets seem to survive in a dormant state according to Levison et al., 2002), disintegration is likely not the explanation for the disappearance of JFCs or their final fate.

In the previous section we showed that the slope of the H-distribution of dormant JFCs is $\alpha = 0.30 \pm 0.06$ (combined statistical and systematic error). This value is in agreement with that determined by Levison et al. (2002) for a sample of 9 dormant HTCs ($\alpha_{\rm HTC} = 0.23 \pm 0.04$) despite the different fading behaviors of the two types of comets as described in the last paragraph.

As we stated in the introduction, it is instructive to compare the size distribution of active and dormant comets. Unfortunately, measuring the SFD of active comets or, equivalently, the H-magnitude distribution of their *nuclei*, is a daunting task. Since comets are small they are easiest to observe when closest to Earth, but at this heliocentric distance they develop comae that mask their nuclei and can increase their brightnesses by up to 10 magnitudes (Fernández et al., 1999). (See Lamy et al. (2004) for a recent review and compilation of cometary nuclei.)

The observation of an active comet leads, with some assumption of the dependence of its activity on the heliocentric distance, to an estimate of the comet's *total absolute magnitude*, often denoted $H_{\rm T}$ or H_{10}. This is a measure of the intrinsic brightness of the combined nucleus and coma. Some studies have attempted to physically model the coma in order to subtract its contribution to the overall brightness profile and reveal the bare nucleus (discussed in detail in Tancredi et al., 2000). This method involves modeling light scattered by dust grains and gas (due to sublimation from the surface) ejected from the nucleus. The modeling process is difficult and different coma profiles yield various estimates of the nucleus' brightness. Fernández et al. (1999) found that for very active comets $H_{\rm T}$ scales as $0.75 H_{\rm N}$, while for low-activity comets it scales as $1.5 H_{\rm N}$. $H_{\rm N}$ is the absolute magnitude of the bare nucleus, or the absolute magnitude that the comet would have if it had no activity. It can be identified as the absolute magnitude H used throughout this work.

Hughes (2002) reports that the $H_{\rm T}$-distribution of the active bright JFCs ($H_{\rm T} < 6.6$) is $\alpha_{\rm T}({\rm JFC}) = 0.36$. (This value is essentially the same as that determined by the same author for active, bright LPCs; Hughes, 2001.) If one accepts the scaling between $H_{\rm T}$ and H for very active comets reported above, the H-distribution of active JFCs would have an exponent $\alpha_{\rm N}({\rm JFC}) = 0.24$. Fernandez and Morbidelli (work in progress) found that the $H_{\rm T}$ distribution for faint active JFCs has $\alpha_{\rm T}({\rm JFC}) = 0.2$. Using the scaling between $H_{\rm T}$ and H for low-activity comets reported above, this gives $\alpha_{\rm N}({\rm JFC}) = 0.27$. Thus, once again, there is good agreement between the results presented here and other recent work.

Another approach to determining the nuclear SFD involves measuring cometary magnitudes at large heliocentric distances where the comets are presumably inactive (e.g., Meech et al., 2004; Lowry et al., 2003). There are problems with this approach as well since cometary nuclei are very faint at large heliocentric distances and magnitude measurements are affected by sky brightness and seeing. It is also known that some comets remain active up to many AU from the Sun, and that this residual activity is often difficult to detect due to the small angle subtended by a distant comet on the sky.

One stab at the problem involves comparing a comet's profile with a stellar PSF. If the comet is extended compared to the point source then it is considered to have a coma which can then be modeled and subtracted away (Licandro et al., 2000). This method will not be effective for comets so far away that they are completely contained within a pixel—e.g., a comet located at 10 AU with a 7200-km-diameter coma (∼8 orders of magnitude larger in volume than the typical nucleus) subtends only 1″. Thus, even very large comae that contribute dramatically to the apparent brightness of a distant comet can go unnoticed.

Using the coma modeling and subtraction approach, Fernández et al. (1999) found that the H-distribution of JFCs has $\alpha = 0.53 \pm 0.05$ over a very narrow magnitude range corresponding to nuclear radii of 2–4 km. Weissman and Lowry (2003) found $\alpha = 0.32 \pm 0.01$ in the 1–10 km range while Meech et al. (2004) found $\alpha = 0.290 \pm 0.010$ in the same range and $\alpha = 0.382 \pm 0.012$ in the sub-range from 2 to 5 km. Lamy et al. (2004) summarized all these results in their Table 6 where they also report an updated value for the Weissman and Lowry (2003) paper by Weissman of $\alpha = 0.36 \pm 0.01$. Furthermore, Lamy et al. (2004) performed their own analysis of the cumulative data on cometary nuclei and found $\alpha = 0.38 \pm 0.06$ for

nuclei >3.2 km in diameter. These may be compared to our result of $\alpha = 0.30 \pm 0.06$ for dormant cometary nuclei diameters in the range 0.25–15 km (assuming a 0.04 albedo typical of cometary nuclei; Fernández et al., 2001). It is interesting to note that the two studies with largest number of objects have the largest reported errors on their slopes.

It should be pointed out that the bulk of the JFC candidates on which we have based our study have $16 < H < 21$ corresponding to radii between 0.1 and 2 km. Thus, our α applies to a size range that is not really addressed by the studies of active comet SFDs mentioned above, except in the preliminary Fernandez and Morbidelli work. Despite all the uncertainties, the convergence and agreement of all the slope measurements using different techniques (except for the single result of Fernández et al., 1999) gives an indication that the SFD of active comets is shallow.

Keeping all these caveats in mind, the similarity between the SFD of active and dormant comets suggests that in the fading process the probability of becoming dormant versus disintegrating is roughly size-independent. This seems to be true both when comets in the majority become dormant (as in the JFC case) and when they most likely disrupt (as in the LPC/HTC case).

This conclusion can guide us to an understanding of why the SFD of *active* comets is shallow. In essence, there are two possible interpretations. Either (i) the SFD of comets in the reservoirs (scattered disk, Oort cloud) is as shallow as observed for active comets, or (ii) the SFD of active comets is shallower than that in the parent reservoirs as a consequence of a size-dependent fading probability. The fact that the SFD of dormant comets is similar to that of active comets tends to support (i) against (ii). The reason is simple. Imagine the case that comets have a size-dependent fading probability and that all faded comets are dormant. Then, the SFD of active comets would appear shallower than the parent SFD, but the SFD of dormant comets would appear *steeper*. The same happens in the case where a size-independent fraction of faded comets become dormant. Thus, scenario (ii) requires that the probability of remaining active and the probability of becoming dormant have the same size-dependence in order that both active and dormant populations have the same SFDs. There is no physical reason for this to be true so if it was it would be a striking coincidence. Thus we prefer scenario (i) as an explanation for the shallow cometary SFD.

The difficulty is that scenario (i) raises the problem of explaining why the populations in the comet reservoirs are shallow. Both the scattered disk and the Oort cloud preserve a fraction of the population of planetesimals initially in the protoplanetary disk through which the giant planets migrated (Dones et al., 2004). Thus, although the current collisional activity inside the comet reservoirs is minimal, originally the comets had to belong to a massive small body population where the collisional evolution had to be intense (at least during the initial phase of transport towards the scattered disk/Oort cloud; see Stern and Weissman, 2001 and Charnoz and Morbidelli, 2003), and thus their SFD had to be close to that of a population at collisional equilibrium. It is now known that, because the impact strength of the planetesimals is size-dependent and has a minimum at about 100 m in radius (Benz and Asphaug, 1999), the equilibrium size distribution is very shallow in the range 100 m–5 km. In fact, according to the SDSS survey (Ivezić et al., 2001) the main asteroid belt (the best example we have of a small body reservoir in collisional equilibrium), has an H-distribution with $\alpha \sim 0.26$ in the range between 300 m and 5 km in diameter. Thus, it is plausible that the SFD of active comets is representative of the SFD in the scattered disk and in the Oort cloud, which in turn are both a fossil remnant of the shallow SFD in the original protoplanetary disk. The Kuiper belt might have also a similarly shallow SFD in the same size range (Pan and Sari, 2005).

If this is true, the SFD of comets should become steep again below 100 m in size. We do not have any direct observational evidence of the populations of active and dormant JFCs in favor or against this prediction. These bodies are simply too faint to detect. However, the paucity of small primary craters on Europa (Bierhaus, E.B., Chapman, C.R., Merline, W.J., 2005. Secondary craters on Europa and implications for cratered surfaces. Preprint), suggests that the SFD of comets remains shallow below 100 m in size. A favored explanation is that objects below this size threshold cannot stand the thermal shocks suffered as they approach within 5–10 AU of the Sun, and therefore disintegrate before they evolve into Jupiter crossing orbits. If this is true, we need to modify the scenario above as follows.

The cometary activity of the large Centaur Chiron suggests that as comet precursors penetrate into the centaur region (non-Jupiter crossing orbits with $5.2 < a < 30$ AU) they experience thermal loads that induce sublimation of volatile ices (e.g., N_2, CO, CH_4, H_2CO, NH_3, CO_2; see Delsemme, 1982). In order to explain our results we propose that there exists a size-dependent disintegration of the precursor objects before they become 'comets.' We will not speculate deeply on the physical mechanism of disruption but point out that the repeated and increasing thermal pulses suffered by the objects as they dynamically evolve closer to the Sun might induce internal mechanical stresses. The smaller the initial object, the more likely it may be to disrupt under the thermal-induced stresses that it is experiencing for the first time. Consequently, the population of bodies smaller than 100 m is annihilated and the SFD of the larger survivors might become somewhat shallower than the SFD of the parent population. The bodies that have passed this initial decimation are strong enough to be able to penetrate closer to the Sun, develop cometary activity for some perihelion passages, and finally form a crust of refractory material that eventually makes them dormant.

This scenario is different from the scenario (ii) that we have rejected above. Scenario (ii) was invoking a size-dependent fading probability. This scenario requires a size-dependent disruption probability before the beginning of classical cometary activity. Then, for the comets that pass this first selection and develop cometary activity, it invokes a size-independent fading to the dormant state as given in scenario (i). This new scenario (i′) would explain the shallow SFD of active JFCs, the equally shallow SFD of dormant JFCs and the paucity of small primary craters on Jupiter's satellites. It is a little bit more problematic

to explain why the SFDs of the active LPCs and the dormant HTCs are also similar.

With the currently available data, it is difficult to discriminate between scenarios (i) and (i′). To break the degeneracy between the two requires additional information in the form of (a) the detection of smaller active/dormant comets in order to extend the SFD, and (b) an in situ detailed analysis of the crater SFD on the distant icy satellites of all giant planets and Kuiper belt objects.

5. Conclusion

We have identified a set of 61 NEOs that are likely to be the dormant nuclei of JFCs and modeled their observational selection effects in order to determine the slope of their actual absolute-magnitude frequency distribution: $\alpha = 0.30 \pm 0.03$ (stat) ± 0.05 (sys). The total number of dormant JFCs with $H < 18$ in the NEO region is ∼75 and the completion rate in the known data sample for objects in this size range is about 30%. The slope for the HFD as determined by our novel method is consistent with most other recent measures of the same quantity that used different techniques (e.g., Fernández et al., 1999; Weissman and Lowry, 2003; Meech et al., 2004). Our results push the HFD to a smaller size range than have been published and are also applicable over a wider range than previous work. The estimate for the total number of dormant JFCs is consistent with other estimates (Bottke et al., 2002a).

Our results suggest a physical and dynamical evolutionary scenario as follows:

- the SFD of comets in their reservoirs (scattered disk, Oort cloud) is shallow and a remnant of their equilibrium SFD within the protoplanetary disk before being scattered, *or*
- the SFD of comets in their reservoirs is somewhat shallow and as the comet precursors penetrate into the giant planet region (non-Jupiter crossing orbits with $5.2 < a < 30$ AU) they suffer strong thermal stresses that induce a size-dependent disintegration probability before they become ‘comets.’ Objects smaller than 100-m-diameter are effectively annihilated and the SFD of the survivors will be shallower than the SFD of the parent population; *then*
- the objects penetrate closer to the Sun, develop cometary activity for some perihelion passages, and finally form a crust of refractory material that eventually makes them dormant. All these processes proceed in a size-independent manner.

These scenarios explain the observed shallow SFD of active JFCs, the equally shallow SFD of dormant JFCs (this work and, e.g., Fernández et al., 1999; Weissman and Lowry, 2003; Meech et al., 2004) and the paucity of small primary craters on Jupiter’s satellites (Bierhaus, E.B., Chapman, C.R., Merline, W.J., 2005. Secondary craters on Europa and implications for cratered surfaces. Preprint).

Future studies involving the detection and characterization of smaller active/dormant comets, and in situ analysis of the crater SFD on the distant icy satellites of all giant planets and Kuiper belt objects will provide the litmus test for deciding if this scenario is realistic.

Acknowledgments

We thank Bill Bottke, Yanga Fernández, Hal Levison, and Nalin Samarasinha for helpful discussions interpreting the results of this study. Paul Weigert and Philippe Lamy provided constructive reviews.

References

Benz, W., Asphaug, E., 1999. Catastrophic disruptions revisited. Icarus 142, 5–20.

Binzel, R.P., Rivkin, A.S., Stuart, J.S., Harris, A.W., Bus, S.J., Burbine, T.H., 2004. Observed spectral properties of near-Earth objects: Results for population distribution, source regions, and space weathering processes. Icarus 170, 259–294.

Bottke, W.F., Jedicke, R., Morbidelli, A., Petit, J., Gladman, B., 2000. Understanding the distribution of near-Earth asteroids. Science 288, 2190–2194.

Bottke, W.F., Morbidelli, A., Jedicke, R., Petit, J., Levison, H.F., Michel, P., Metcalfe, T.S., 2002a. Debiased orbital and absolute magnitude distribution of the near-Earth objects. Icarus 156, 399–433.

Bottke, W.F., Vokrouhlický, D., Rubincam, D.P., Broz, M., 2002b. The effect of Yarkovsky thermal forces on the dynamical evolution of asteroids and meteoroids. In: Bottke Jr., W.F., Cellino, A., Paolicchi, P., Binzel, R. (Eds.), Asteroids III. Univ. of Arizona Press, Tucson, pp. 395–408.

Bottke, W.F., Durda, D.D., Nesvorný, D., Jedicke, R., Morbidelli, A., Vokrouhlický, D., Levison, H., 2005. The fossilized size distribution of the main asteroid belt. Icarus 175, 111–140.

Campo Bagatin, A., Cellino, A., Davis, D.R., Farinella, P., Paolicchi, P., 1994. Wavy size distributions for collisional systems with a small-size cutoff. Planet. Space Sci. 42, 1079–1092.

Charnoz, S., Morbidelli, A., 2003. Coupling dynamical and collisional evolution of small bodies: An application to the early ejection of planetesimals from the Jupiter–Saturn region. Icarus 166, 141–156.

Delsemme, A.H., 1982. Chemical composition of cometary nuclei. In: Wilkenning, L.L. (Ed.), Comets. Univ. of Arizona Press, Tucson, pp. 85–130.

Dohnanyi, J.W., 1969. Collisional models of asteroids and their debris. J. Geophys. Res. 74, 2531–2554.

Dones, L., Weissman, P.R., Levison, H.F., Duncan, M.J., 2004. Oort cloud formation and dynamics. In: Festou, M.C., Keller, H.U., Weaver, H.A. (Eds.), Comets II. Univ. of Arizona Press, Tucson, pp. 153–174.

Durda, D.D., 1993. The collisional evolution of the asteroid belt and its contribution to the zodiacal cloud. Appendix B. Ph.D. thesis, University of Florida.

Durda, D.D., Greenberg, R., Jedicke, R., 1998. Collisional models and scaling laws: A new interpretation of the shape of the main-belt asteroid size distribution. Icarus 135, 431–440.

Fernandez, J.A., 1981. New and evolved comets in the Solar System. Astron. Astrophys. 96, 26–35.

Fernández, J.A., Tancredi, G., Rickman, H., Licandro, J., 1999. The population, magnitudes, and sizes of Jupiter family comets. Astron. Astrophys. 352, 327–340.

Fernández, Y.R., Jewitt, D.C., Sheppard, S.S., 2001. Low albedos among extinct comet candidates. Astrophys. J. 553, L197–L200.

Hughes, D.W., 2001. The magnitude distribution, perihelion distribution and flux of long-period comets. Mon. Not. R. Astron. Soc. 326, 515–523.

Hughes, D.W., 2002. The magnitude distribution and evolution of short-period comets. Mon. Not. R. Astron. Soc. 336, 363–372.

Ivezić, Ž., and 32 colleagues, 2001. Solar System objects observed in the Sloan Digital Sky Survey commissioning data. Astrophys. J. 122, 2749–2784.

Jedicke, R., Metcalfe, T.S., 1998. The orbital and absolute magnitude distributions of main belt asteroids. Icarus 131, 245–260.

Jedicke, R., Larsen, J., Spahr, T., 2002. Observational selection effects in asteroid surveys. In: Bottke Jr., W.F., Cellino, A., Paolicchi, P., Binzel, R. (Eds.), Asteroids III. Univ. of Arizona Press, Tucson, pp. 71–87.

Jedicke, R., Morbidelli, A., Spahr, T., Petit, J., Bottke, W.F., 2003. Earth and space-based NEO survey simulations: Prospects for achieving the space-guard goal. Icarus 161, 17–33.

Kuiper, G.P., Fugita, Y.F., Gehrels, T., Groeneveld, I., Kent, J., van Biesbroeck, G., van Houten, C.J., 1958. Survey of asteroids. Astrophys. J. Suppl. Ser. 3, 289.

Lamy, P.L., Toth, I., Fernandez, Y.R., Weaver, H.A., 2004. The sizes, shapes, albedos, and colors of cometary nuclei. In: Festou, M.C., Keller, H.U., Weaver, H.A. (Eds.), Comets II. Univ. of Arizona Press, Tucson, pp. 223–264.

Levison, H.F., Duncan, M.J., 1997. From the Kuiper belt to Jupiter-family comets: The spatial distribution of ecliptic comets. Icarus 127, 13–32.

Levison, H.F., Morbidelli, A., Dones, L., Jedicke, R., Wiegert, P.A., Bottke, W.F., 2002. The mass disruption of Oort cloud comets. Science 296, 2212–2215.

Licandro, J., Tancredi, G., Lindgren, M., Rickman, H., Hutton, R.G., 2000. CCD photometry of cometary nuclei. I. Observations from 1990–1995. Icarus 147, 161–179.

Lowry, S.C., Fitzsimmons, A., Collander-Brown, S., 2003. CCD photometry of distant comets. III. Ensemble properties of Jupiter-family comets. Astron. Astrophys. 397, 329–343.

Lyons, L., 1986. Statistics for Nuclear and Particle Physicists. Cambridge Univ. Press, Cambridge, pp. 85–98.

Meech, K.J., Hainaut, O.R., Marsden, B.G., 2004. Comet nucleus size distributions from HST and Keck telescopes. Icarus 170, 463–491.

Morbidelli, A., Vokrouhlický, D., 2003. The Yarkovsky-driven origin of near-Earth asteroids. Icarus 163, 120–134.

Pan, M., Sari, R., 2005. Shaping the Kuiper belt size distribution by shattering large but strengthless bodies. Icarus 173, 342–348.

Stern, S.A., Weissman, P.R., 2001. Rapid collisional evolution of comets during the formation of the Oort cloud. Nature 409, 589–591.

Tanaka, H., Inaba, S., Nakazawa, K., 1996. Steady-state size distribution for the self-similar collision cascade. Icarus 123, 450–455.

Tancredi, G., Fernández, J.A., Rickman, H., Licandro, J., 2000. A catalog of observed nuclear magnitudes of Jupiter family comets. Astron. Astrophys. Suppl. 146, 73–90.

van Houten, C.J., van Houten-Groeneveld, I., Herget, P., Gehrels, T., 1970. The Palomar–Leiden survey of faint minor planets. Astron. Astrophys. Suppl. 2, 339–448.

Weissman, P.R., 1978. Physical and dynamical evolution of long-period comets. Ph.D. thesis.

Weissman, P.R., Lowry, S.C., 2003. The size distribution of Jupiter-family cometary nuclei. Lunar Planet. Sci. 34. Abstract 2003.

Wiegert, P., Tremaine, S., 1999. The evolution of long-period comets. Icarus 137, 84–121.